

Zn-triggered critical behavior of the formation of highly coherent domains in a $\text{Mg}_{1-x}\text{Zn}_x\text{O}$ thin film on Al_2O_3

Chinkyoo Kim* and Shi-Jong Leem

Optoelectronics Group, LG Electronics Institute of Technology, 16 Woomyeon-dong, Seocho-gu, Seoul 137-724, Korea

Ian K. Robinson

Department of Physics, University of Illinois at Urbana-Champaign, 1110 W. Green St., Urbana, IL 61801

W. I. Park, D. H. Kim, and G. -C. Yi

Department of Materials Science and Engineering, Pohang University of Science and Technology (POSTECH), Pohang 790-784, Korea

(Received 25 January 2002; revised manuscript received 11 April 2002; published 23 September 2002)

A series of $\text{Mg}_{1-x}\text{Zn}_x\text{O}$ ($x=0, 0.05, 0.10$, and 0.15) thin films were grown by metal-organic chemical vapor deposition on a (0001) sapphire substrate, and the structural characteristics of $\text{Mg}_{1-x}\text{Zn}_x\text{O}$ thin films were investigated by synchrotron x-ray diffraction. The increasing amount of Zn was found to gradually enhance the structural coherence of $\text{Mg}_{1-x}\text{Zn}_x\text{O}$ films. For a sample with 15 at. % of Zn, in particular, the formation of highly coherent domains in $\text{Mg}_{1-x}\text{Zn}_x\text{O}$ was observed to be triggered, with an accompanying phase separation of ZnO. An integrated intensity analysis predicted that the critical concentration x_c of Zn at which the phase separation occurred was 0.086 ± 0.015 , and that the highly coherent domains in $\text{Mg}_{1-x}\text{Zn}_x\text{O}$ accounted for $12 \pm 1\%$.

DOI: 10.1103/PhysRevB.66.113404

PACS number(s): 61.10.-i, 68.35.Rh, 68.60.-p, 73.61.Ey

With the recent development of GaN-based optoelectronic devices, various other wide band gap materials are extensively investigated to fabricate short wavelength optoelectronic devices with better performance. ZnO is among the most promising candidates for this purpose since it has a large exciton binding energy (~ 60 meV) and bond strength. In particular, recent studies of ZnO showed that the extremely stable excitons survived well above room temperature, implying the possibility of low-threshold excitonic lasers.^{1,2}

Lately, Ohtomo *et al.* reported that the band gap of ZnO was enlarged by alloying with MgO,³ and the growth and characterization of $\text{Zn}_{1-x}\text{Mg}_x\text{O}$ alloy for band gap engineering have become key issues to construct various optical and electrical devices. The research on $\text{Zn}_{1-x}\text{Mg}_x\text{O}$ alloy has, however, been very limited partly due to only a few growth methods available such as pulsed laser deposition or molecular beam epitaxy. Our previous work showed that high quality $\text{Zn}_{1-x}\text{Mg}_x\text{O}$ could be grown by metal-organic vapor phase epitaxy.⁴

In this work, we extended our work to investigate the structural characteristics of $\text{Mg}_{1-x}\text{Zn}_x\text{O}$ film on a (0001) sapphire substrate utilizing a synchrotron x-ray diffraction, and the very intriguing effect of incorporated Zn on the structural coherence of $\text{Mg}_{1-x}\text{Zn}_x\text{O}$ was observed. A series of $\text{Mg}_{1-x}\text{Zn}_x\text{O}$ ($x=0, 0.05, 0.10$, and 0.15) thin films were grown on a (0001) sapphire substrate by metal-organic chemical vapor deposition. Bis-cyclopentadienylmagnesium (Cp_2Mg), diethylzinc (DEZn), and oxygen were used as Mg, Zn, and O sources, respectively. The growth temperature and reactor pressure were maintained constant at 600°C and 5 torr, respectively. The thickness of the films was measured to be 1300 \AA , and the thickness variation with Zn contents was negligible. The amount of Zn incorporated into MgO was

controlled by the DEZn flow rate, and the atomic percentage of Zn was determined by energy dispersive x-ray spectroscopy. X-ray diffraction experiments utilizing a synchrotron radiation source were performed at beamline X16C of National Synchrotron Light Source at Brookhaven National Laboratory. A double crystal Si(111) monochromator produced x rays of 11.5 keV ($\lambda = 1.0781 \text{ \AA}$). A four circle diffractometer featuring *kappa geometry*⁵ was used for measurement. Our experimental resolution was determined by a $1 \times 2\text{-mm}^2$ wide slits in front of a scintillation detector.

MgO and ZnO have rocksalt and wurtzite structures, respectively. Since they have a different coordination number and crystal symmetry, it is expected that Zn will replace Mg without changing the original structure up to a certain amount when alloying. According to the phase diagram, MgO allows a maximum of 56% ZnO (wt %, 40 at. %) at 1600°C , and maintains its NaCl structure with the lattice constant staying close to that of pure MgO 4.208 \AA ,⁶ but it does not necessarily mean that $\text{Mg}_{1-x}\text{Zn}_x\text{O}$ with x up to 0.4 is a stable phase at room temperature.

As far as the orientational relation is concerned, our x-ray-diffraction result showed that cubic $\text{Mg}_{1-x}\text{Zn}_x\text{O}$ thin films were epitaxially grown with the orientational relationship of $\text{Mg}_{1-x}\text{Zn}_x\text{O}(111) \parallel \text{Al}_2\text{O}_3(0001)$, $\text{Mg}_{1-x}\text{Zn}_x\text{O}[\bar{1}10] \parallel \text{Al}_2\text{O}_3[10\bar{1}0]$ in all of our samples, and that the lattice parameters were not markedly changed from those of MgO through the samples implying that the films were fully relaxed. The ϕ scan in Fig. 1 showed, however, a sixfold symmetry, signifying that there were either 60° twins or inversion domains of $\text{Mg}_{1-x}\text{Zn}_x\text{O}$ because only threefold symmetry is allowed for a (200) Bragg peak in a single domain $\text{Mg}_{1-x}\text{Zn}_x\text{O}$.

For a large lattice-mismatched system such as MgO on sapphire with $\sim 8.4\%$ lattice mismatch, it is common for

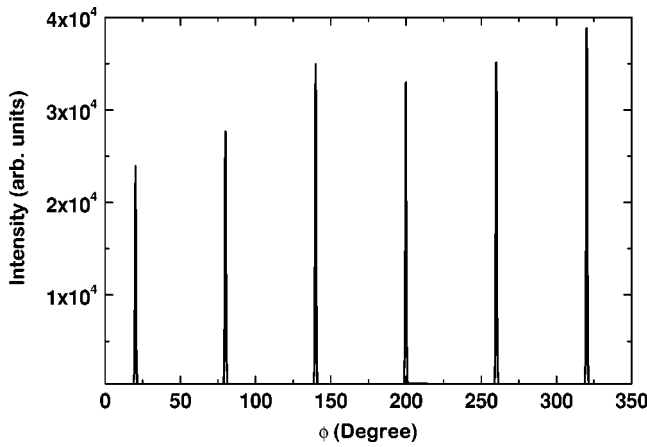


FIG. 1. The ϕ scan through $\text{Mg}_{1-x}\text{Zn}_x\text{O}$ (200) Bragg peaks shows that there are either 60° twins or inversion domains in the film.

dislocations to induce rotational disorder in order to relieve strain. This type of rotational disorder can usually be characterized by the x-ray rocking curve measurement. As for the out-of-plane rotational disorder, θ rocking curves of a $\text{Mg}_{1-x}\text{Zn}_x\text{O}$ (111) Bragg peak were measured, and a gradual decrease of the Bragg peak width was observed with the increasing amount of Zn. As shown in Fig. 2, a very narrow component on top of a broad peak was, however, found in the sample with 15% of Zn. (Data were plotted as a function of the surface parallel component of the momentum transfer vector instead of $\Delta\theta$. This unit conversion is valid for a small value of $\Delta\theta$ with a good approximation.) For a θ rocking curve of $\text{Mg}_{1-x}\text{Zn}_x\text{O}$ (222) in the same sample, there was only a broad peak with no such a sharp peak on top of it. Note that the width of the diffuse component for (111) and (222) is not dependent upon the magnitude of the momentum transfer vector. This seemingly peculiar rocking profile cannot be explained by a simple *mosaicity* model because it predicts the same angular width of each Bragg peak with no narrow component.

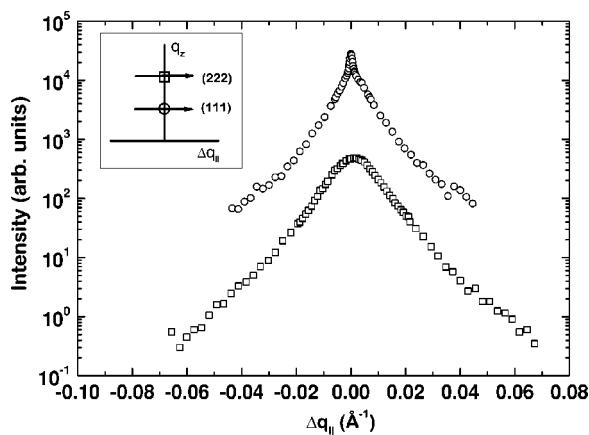


FIG. 2. The θ rocking scan of the (111) Bragg peak of 15% of a Zn-incorporated $\text{Mg}_{1-x}\text{Zn}_x\text{O}$ thin film. A two-line shape rocking profile was observed only for this sample. Data were plotted as a function of the surface parallel component of the momentum transfer vector instead of $\Delta\theta$.

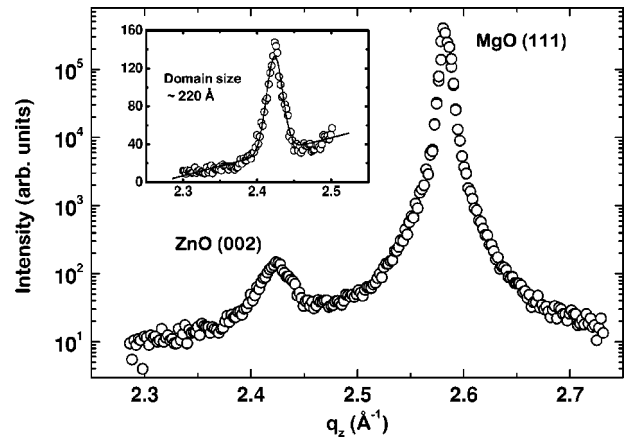


FIG. 3. The θ - 2θ scan of 15% of a Zn-incorporated $\text{Mg}_{1-x}\text{Zn}_x\text{O}$ thin film clearly shows a ZnO phase with an inset of a Gaussian fit to a ZnO(002) Bragg peak. The average grain size is estimated to be ~ 220 Å from the Scherrer formula.

The coexistence of narrow and diffuse component is well known from the scattering theory for disordered crystalline solids, where the narrow component arises from the long-range order and is attenuated by the uncorrelated disorder, whereas the broad component comes from the short-range correlations.⁷ Thus, two-line shape rocking profile of $\text{Mg}_{1-x}\text{Zn}_x\text{O}$ at $x=0.15$ implies that there are highly ordered coherent $\text{Mg}_{1-x}\text{Zn}_x\text{O}$ domains embedded in a mostly less ordered $\text{Mg}_{1-x}\text{Zn}_x\text{O}$ matrix. Due to the very nature of epitaxy, the highly ordered $\text{Mg}_{1-x}\text{Zn}_x\text{O}$ domains are most likely to be formed at the interface region, maintaining its coherence with the substrate. The fact that the full widths at half maximum (FWHM) of (111) Bragg peak from these domains are comparable to that of the sapphire (006) Bragg peak is indirect evidence which supports this assertion.

As for the role of Zn in assisting the formation of highly ordered $\text{Mg}_{1-x}\text{Zn}_x\text{O}$ domains, it is worthwhile to investigate any critical behavior of the Zn-related phase around a 15% Zn-incorporated sample. In order to see if there was any phase separation in our samples, θ - 2θ scans along the surface normal direction were carried out. No signature of ZnO phase separation in the samples with up to 10% Zn incorporation was found. For the sample with 15% of Zn, however, the ZnO phase was observed (Fig. 3) with an average grain size of ~ 220 Å estimated by the Scherrer formula

$$D \approx \frac{0.9\lambda}{(2\theta)_{\text{FWHM}} \cos \theta}, \quad (1)$$

where D is the domain size, and θ is the angle of the Bragg peak. From our data, it seems that the formation of coherent domains of $\text{Mg}_{1-x}\text{Zn}_x\text{O}$ is observed to be triggered only above a critical concentration of incorporated Zn, and that ZnO phase separation also takes place approximately at the same critical level of incorporated Zn.

In order to understand Zn-triggered critical phenomena more quantitatively, we propose a model to explain our experimental results in the following. Up to a critical concentration (x_c) of Zn, Zn is homogeneously mixed in

$\text{Mg}_{1-x}\text{Zn}_x\text{O}$. If more than a critical concentration of Zn, ($x_o \geq x_c$) is incorporated at a growth temperature, $\text{Mg}_{1-x_o}\text{Zn}_{x_o}\text{O}$ will decompose to $\text{Mg}_{1-x_c}\text{Zn}_{x_c}\text{O}$ and ZnO at room temperature to lower the total energy of the film. Based on this model, we calculated the integrated intensities of the Bragg peaks [$\text{Mg}_{1-x}\text{Zn}_x\text{O}(111)$ and $\text{ZnO}(002)$] to verify that our model is consistent with the experimental results.

To calculate the integrated intensity of a specific component of a Bragg peak, we need to figure out how many unit cells in each phase contribute to the corresponding component. If the number of unit cells in $\text{Mg}_{1-x_o}\text{Zn}_{x_o}\text{O}$ is N_o , then the number of unit cells in $\text{Mg}_{1-x_c}\text{Zn}_{x_c}\text{O}$ and ZnO after the decomposition of $\text{Mg}_{1-x_o}\text{Zn}_{x_o}\text{O}$, N_c and N_z , can be related as follows because there are only two Zn atoms in one unit cell of wurtzite structure if we assume that the number of Mg and Zn atoms in the film are conserved even after the decomposition:

$$(1-x_o)N_o = (1-x_c)N_c, \quad (2)$$

$$N_c \equiv 2(x_o N_o - x_c N_c) = 2(N_o - N_c). \quad (3)$$

Then a certain amount of $\text{Mg}_{1-x_c}\text{Zn}_{x_c}\text{O}$ phase will be in a highly ordered state, and we label this ratio α . Thus the number of unit cells in $\text{Mg}_{1-x_c}\text{Zn}_{x_c}\text{O}$ contributing to the narrow and broad components of the $\text{Mg}_{1-x_c}\text{Zn}_{x_c}\text{O}$ (111) Bragg peak, N_{narrow} and N_{broad} , can be related to N_o , using Eqs. (2) and (3), as

$$\frac{N_z}{N_{\text{narrow}}} \equiv \frac{N_z}{\alpha N_c} = \frac{2(x_o - x_c)}{\alpha(1-x_o)}, \quad (4)$$

$$\frac{N_z}{N_{\text{broad}}} \equiv \frac{N_z}{(1-\alpha)N_c} = \frac{2(x_o - x_c)}{(1-\alpha)(1-x_o)}. \quad (5)$$

Other factors we need to consider to calculate the integrated intensity are the atomic form factors and structure factors of each unit cell. Atomic form factors can be calculated using an analytical expression of

$$f\left(\frac{\sin \theta}{\lambda}\right) = \sum_{i=1}^4 a_i \exp\left[-b_i \frac{\sin^2 \theta}{\lambda^2}\right] + c, \quad (6)$$

and the tabulated constants a_i , b_i , and c for each element,¹⁵ and are given by $f_{\text{Mg}} = 8.655$, $f_{\text{Zn}} = 24.071$, and $f_{\text{O}} = 5.530$ at $\theta = 12.8^\circ$ [corresponding to the Bragg condition for $\text{Mg}_{1-x}\text{Zn}_x\text{O}$ (111) where we assumed that the Bragg condition did not change significantly with different Zn concentrations], and $f_{\text{Zn}} = 24.531$, $f_{\text{O}} = 5.744$ at $\theta = 12.0^\circ$ [corresponding to the Bragg condition for ZnO (002)]. Combining the atomic form factors, the structure factors of $\text{Mg}_{1-x}\text{Zn}_x\text{O}$ and ZnO are given by $|F_{\text{Mg}_{1-x}\text{Zn}_x\text{O}}| = 61.664x + 12.5$ at $\theta = 12.8^\circ$, and $|F_{\text{ZnO}}| = 50.389$ at $\theta = 12.0^\circ$.

Since the integrated intensity I is proportional to the structure factor and the number of unit cells, we end up with the expressions from Eqs. (4) and (5) with the structure factors

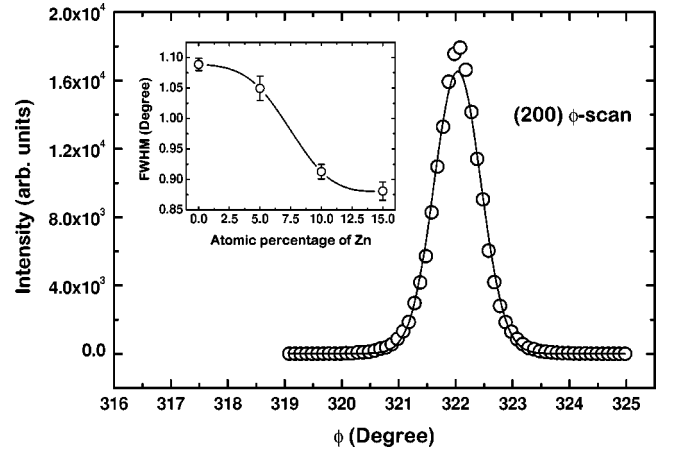


FIG. 4. The typical ϕ scan of a $\text{Mg}_{1-x}\text{Zn}_x\text{O}$ (200) Bragg peak. The inset shows the monotonic decrease of the full width at half maximum values as a function of the incorporated amount of Zn. The solid line in the inset is a guide to the eyes.

$$\sqrt{\frac{I_{\text{ZnO}}}{I_{\text{narrow}}}} = \frac{2(x_o - x_c)}{\alpha(1-x_o)} \left[\frac{50.389}{61.664x_c + 12.5} \right], \quad (7)$$

$$\sqrt{\frac{I_{\text{ZnO}}}{I_{\text{broad}}}} = \frac{2(x_o - x_c)}{(1-\alpha)(1-x_o)} \left[\frac{50.389}{61.664x_c + 12.5} \right]. \quad (8)$$

From our measurements, the ratios of the integrated intensities between each component are given by $I_{\text{ZnO}}/I_{\text{narrow}} = 3.52^2$ and $I_{\text{ZnO}}/I_{\text{broad}} = 0.474^2$. Plugging these numbers and $x_o = 0.15$ into Eqs. (7) and (8), we obtain $\alpha = 0.12 \pm 0.01$ and $x_c = 0.086 \pm 0.015$. This implies that $\text{Mg}_{1-x_o}\text{Zn}_{x_o}\text{O}$ with $x_o = 0.15 \geq x_c = 8.6 \pm 1.5$ decompose to $\text{Mg}_{1-x_c}\text{Zn}_{x_c}\text{O}$ and ZnO, and that only approximately 12% of a $\text{Mg}_{1-x_c}\text{Zn}_{x_c}\text{O}$ phase will contribute to the narrow component of the Bragg peak. The integrated intensity analysis based on our model is in excellent agreement with the fact that we could not observe any ZnO phase separation for samples where the Zn concentration is less than 10%, and is also consistent with our qualitative interpretation above that only a small portion of highly ordered domains are embedded in a less ordered matrix.

In addition to out-of-plane ordering, we also expected that in-plane domain ordering took place by Zn incorporation. For an estimation of rotational disorder in the in-plane direction, ϕ rocking curves were measured for the $\text{Mg}_{1-x}\text{Zn}_x\text{O}(200)$ Bragg peak. In Fig. 4, a typical ϕ rocking curve for a (200) $\text{Mg}_{1-x}\text{Zn}_x\text{O}$ film is shown with an inset showing a monotonic decrease of rotational disorder in the in-plane direction as a function of the amount of Zn incorporation. The incorporation of Zn assists the ordering of $\text{Mg}_{1-x}\text{Zn}_x\text{O}$ domains in the in-plane direction as well. The incorporated Zn above a critical value not only influenced the structural coherence, but also greatly enhanced the surface morphology, which was manifested by the appearance of up to tenth-order thickness fringes in the θ - 2θ scan and atomic force microscopy image (data not shown).

This kind of two-line shape rocking profile was also observed in other heteroepitaxial systems such as Nb/Al₂O₃, ErAs/GaAs, and Ti/MgO.⁸⁻¹² Miceli *et al.* successfully explained the dependence of the width of the diffuse component as a function of the momentum transfer vector. Recently, Barabash *et al.* extended the Krivoglaz theory, and were even able to calculate the line *shape* of the diffuse component by modeling the misfit dislocation networks.¹³ In all of the systems mentioned above, the dislocation density was known to be the main source of rotational disorder causing a diffuse component, with the thickness playing a role in determining the dislocation density.

On the other hand, what distinguishes Mg_{1-x}Zn_xO from other systems, even though it showed a similar two-line shape profile, is the fact that the formation of highly ordered domains resulted from incorporated Zn above a critical concentration. In this system, the concentration of incorporated Zn seems to play the same role as the thickness of the film in the systems mentioned above did, triggering highly ordered coherent domains at a critical value. Considering the similarity in radii of Zn²⁺ and Mg²⁺ ions (1.25 and 1.36 Å,

respectively),¹⁴ the incorporated Zn may easily substitute the Mg site up to a certain amount, but a phase separation takes place above a critical concentration. However, the point where the coherent (rocksalt) domains are observed to form is also the concentration at which separate ZnO (wurtzite) domains arose.

In conclusion, the structural ordering of a series of Mg_{1-x}Zn_xO thin films with different atomic percentages of Zn was investigated by synchrotron x-ray diffraction. The effect of Zn incorporation on the structural coherence of the overall Mg_{1-x}Zn_xO film manifested itself gradually, but there was a critical point in the amount of Zn incorporation which triggered the formation of highly ordered domains. An integrated intensity analysis, based on a phase separation model, showed that the critical concentration x_c was 0.086 ± 0.015 and the highly coherent domains in Mg_{1-x}Zn_xO accounted for 12%.

NSLS activities were supported by the U.S. DOE under Grants Nos. DEAC02-98CH10886 and DEFG02-91ER45439.

*Electronic mail: chnkkim@LG-Elite.com

¹Z. K. Tang, G. K. L. Wong, P. Yu, M. Kawasaki, A. Ohtomo, H. Koinuma, and Y. Segawa, *Appl. Phys. Lett.* **72**, 3270 (1998).

²D. M. Bagnall, Y. F. Chen, Z. Zhu, T. Yao, S. Koyama, M. Y. Shen, and T. Goto, *Appl. Phys. Lett.* **70**, 2230 (1997); D. M. Bagnall, Y. F. Chen, Z. Zhu, T. Yao, M. Y. Shen, and T. Goto, *ibid.* **73**, 1038 (1998).

³A. Ohtomo, M. Kawasaki, T. Koida, K. Masubuchi, H. Koinuma, Y. Sakurai, Y. Yoshida, T. Yasuda, and Y. Segawa, *Appl. Phys. Lett.* **72**, 2466 (1998).

⁴W. I. Park, G. C. Yi, and H. M. Jang, *Appl. Phys. Lett.* **79**, 2022 (2001).

⁵I. K. Robinson, H. Graafsma, A. Kvik, and J. Linderholm, *Rev. Sci. Instrum.* **66**, 1765 (1995).

⁶E. R. Segnit and A. E. Holland, *J. Am. Ceram. Soc.* **48**, 412 (1965).

⁷M. A. Krivoglaz, *Theory of X-ray and Thermal-Neutron Scatter-*

ing by Real Crystals (Plenum, New York, 1969).

⁸P. M. Reimer, H. Zabel, C. P. Flynn, and J. A. Dura, *Phys. Rev. B* **45**, 11426 (1992).

⁹A. R. Wildes, R. A. Cowley, R. C. C. Ward, M. R. Wells, C. Janse, L. Wiren, and J. P. Hill, *J. Phys.: Condens. Matter* **10**, L631 (1998).

¹⁰P. F. Miceli and C. J. Palmstrom, *Phys. Rev. B* **51**, 5506 (1995).

¹¹P. F. Miceli, J. Weatherwax, T. Krentsel, and C. J. Palmstrom, *Physica B* **221**, 230 (1996).

¹²M. Huth and C. P. Flynn, *Appl. Phys. Lett.* **71**, 2466 (1997).

¹³R. I. Barabash, W. Donner, and H. Dosch, *Appl. Phys. Lett.* **78**, 443 (2001).

¹⁴A. K. Sharma, J. Narayan, J. F. Muth, C. W. Teng, C. Jin, A. Kvit, R. M. Kolbas, and O. W. Holland, *Appl. Phys. Lett.* **75**, 3327 (1999).

¹⁵*International Tables for Crystallography*, Kynoch Press, Birmingham, England, (1984).